Theor Appl Climatol
DOI 10.1007/s00704-013-0954-5

ORIGINAL PAPER

Seasonal prediction for tropical cyclone frequency around Taiwan using teleconnection patterns

Ki-Seon Choi · Chun-Chieh Wu · Yuqing Wang

Received: 25 December 2012 / Accepted: 13 May 2013

Abstract In this study, a statistical model is developed to predict the frequency of tropical cyclones (TCs) that influence Taiwan in boreal summer. Predictors are derived from large-scale environments from February to May in six regions, including four atmospheric circulation predictors over the western sea and eastern sea of Australia, the subtropical western North Pacific (SWNP), and the eastern sea of North America, and two sea surface temperature predictors in the Southeast Indian Ocean and the North Atlantic. The statistical model is verified based on statistical cross-validation tests and by contrasting the differences in the large-scale environments between high and low TC frequency years hindcasted by the model. The results show the relationships of two atmospheric circulation predictors and one SST predictor around Australia with Antarctic Oscillation (AAO) pattern, as well as the relationships of those in the SWNP and around eastern sea of North America with Pacific/North American teleconnection (PNA) pattern. When the anomalous anticyclone around Australia (positive AAO pattern) and the one over the region from eastern sea of North America and the Aleutian Islands to the SWNP (negative PNA pattern) are both strengthened from February, the trade wind in the equatorial Pacific is intensified and consequently plays an important role in steering TCs towards Taiwan during boreal summer.

K.-S. Choi
National Typhoon Center, Korea Meteorological Administration, Jeju, Korea
e-mail: choiks@kma.go.kr

C.-C. Wu (✉)
Department of Atmospheric Sciences, National Taiwan University, Taipei, Taiwan
e-mail: cwu@typhoon.as.ntu.edu.tw

Y. Wang
International Pacific Research Center and Department of Meteorology, University of Hawaii at Manoa, Honolulu, HI, USA

1 Introduction

Tropical cyclones (TCs) are one of the natural phenomena that bring deadly damages to coastal regions in the western North Pacific. In particular, strong winds, torrential rains, flash floods, and storm surge caused by TCs often result in losses of lives and properties in East Asia. Even though significant progress has been made in both observations and dynamical models, our ability to predict seasonal TC activity on a particular region is still challenging.

The skill for TC forecasting can be improved as forecasters become more experienced, but greater improvement comes more likely from more accurate forecasting tools. Both dynamical and statistical models are used in operational TC forecasts. Generally, empirical statistical methods that incorporate large-scale environmental predictors are widely used for seasonal prediction of TC activity. Gray et al. (1992, 1993, 1994) developed multiple linear regression models to predict seasonal hurricane activity in the North Atlantic using various large-scale environmental predictors. The predictors that have been used in their models include El Niño/Southern Oscillation (ENSO), Quasi-Biennial Oscillation, and western Sahelian rainfall. The development and improvement of statistical models to correctly predict seasonal hurricane activity in this region have been attempted and are still an active area of research (Elsner and Schmertmann 1993; Hess and Elsner 1994; Lehmiller et al. 1997; Klotzbach 2007; Zhou and Cui. 2008, 2011).

Chan et al. (1998, 2001) attempted the seasonal prediction of TC activity in the western North Pacific basin. They developed a skillful statistical prediction model for seasonal TC activity in the western North Pacific using large-scale environmental predictors including (1) sea surface temperature anomalies over the central and eastern Pacific, (2) circulation patterns over Asia and the western Pacific from April of the previous year to March of the current year, (3) trend of the interannual variations in TC activity, and (4)

Published online: 25 July 2013

circulation patterns in the Australian region and South Pacific. More recently, Fan and Wang (2009) tried to predict the increase and decrease of the western North Pacific TC genesis frequency from the preceding year to the current year based on the differences in various large-scale environmental predictors between the preceding year and the current year. Especially, they made an excellent prediction of the TC genesis frequency in 1997 and 1998 (extremely warm and cold ENSO years, respectively), the most extreme years in the western North Pacific TC genesis frequency. Choi et al. (2010) also tried to predict seasonal frequency of western North Pacific TC genesis using teleconnection patterns, such as Antarctic Oscillation (AAO), North Pacific Oscillation, and Siberian High Oscillation in spring. The developments of statistical models for seasonal prediction of TC activity in the western North Pacific have also been carried out by Lee et al. (2007) and Kwon et al. (2007).

In addition to seasonal prediction of basin-wide seasonal TC activity, the development of statistical models for seasonal prediction of regional TC activity is also an active research area because such seasonal prediction is directly related to the potential damages to lives and properties in the targeted regions. Skillful seasonal prediction for regional TC activity is deemed more difficult than that for basin-wide TC activity because in the former case, both TC genesis and track patterns need to be taken into account, which are determined by both the regional atmospheric and oceanic conditions. Liu and Chan (2003) developed a statistical model to predict the seasonal activity of TCs making landfall in southern China based on the projection-pursuit regression technique using large-scale environmental predictors related to ENSO. Wu et al. (2004) divided East Asia and Southeast Asia into four sub-regions (Korea–Japan, China, Indochinese Peninsula, and the Philippines) and tried to predict the seasonal frequency of TC landfalls in each region using Nino-3.4 index. Choi et al. (2009) developed a statistical model to predict the frequency of TCs influencing Korea in summer using the upper-troposphere anomalous circulation pattern in the preceding spring. Chu et al. (2007) have tried to predict the seasonal TC frequency in the vicinity of Taiwan from a multivariate least absolute deviation (Gray et al. 1992) regression model using environmental predictors, such as sea surface temperature, sea level pressure, low-level relative vorticity, precipitable water, and vertical wind shear. In addition to this research, there are a few studies about the seasonal TC frequency in the vicinity of Taiwan (Lu et al. 2010, 2012).

The above studies mostly defined predictors based on correlation analyses between TC activity and various large-scale environments in preceding seasons while also using those predictors to validate the prediction performances of the statistical models. However, the potential influence of predictors on TC activity has not been explained sufficiently. The performance of statistical models is certainly important, but to understand the potential influence of predictors on TC activity is also important.

The objective of this study is to develop a statistical model to predict the frequency of TCs influencing Taiwan during boreal summer using large-scale environmental predictors before summer, and to use these predictors to show how the large-scale environmental predictors lead TCs to influence Taiwan.

The rest of the paper is organized as follows. The data used in this study and analysis methods are described in Section 2. The statistical model used to predict the seasonal frequency of TCs that influence Taiwan is developed in Section 3. The developed statistical model is verified based on statistical cross-validation tests and by detailed analysis of large-scale environments in Section 4. Finally, concluding remarks are presented in Section 5.

2 Data and methodology

2.1 Data

Data of TC activity are obtained from the best track archives of the Regional Specialized Meteorological Center, Tokyo Typhoon Center. The data sets consist of name, position (longitude and latitude locations), and intensity (minimum sea level central pressures and maximum sustained wind speed) of each TC at every 6-h intervals during 1951–2011 (61 years). In this study, TCs are divided into four categories based on their maximum sustained 10-m wind speed (MSWS): tropical depressions (MSWS$<$17 m s^{-1}), tropical storms (17 m s$^{-1}\leq$MSWS$\leq$24 m s^{-1}), severe tropical storms (25 m s$^{-1}\leq$MSWS$\leq$32 m s^{-1}), and typhoons (MSWS$\geq$33 m s^{-1}).

We also use zonal and meridional winds (meters per second) from the National Centers for Environmental Prediction–National Center for Atmospheric Research (NCEP-NCAR) reanalysis (Kalnay et al. 1996; Kistler et al. 2001). The NCEP-NCAR reanalysis dataset has a horizontal resolution of 2.5×2.5 and is available for the period from 1948 to the present. The NOAA Extended Reconstructured monthly sea surface temperature (SST) obtained from NCEP is also used (Reynolds et al. 2002). This SST dataset has a horizontal resolution of 2.0°×2.0° and is available for the period from 1854 to the present.

2.2 Methodology

In this study, El Niño and La Niña years are defined as SST anomaly$\geq$0.5 °C and SST anomaly$\leq-$0.5 °C, respectively, in the Niño-3.4 region (5°S–5°N, 120°W–170°W). The

climotological SST for SST anomaly is the one averaged during 61 years.

To calculate the TC passage frequency, each TC position is binned into a corresponding 5×5 grid box, and a TC is only counted once even though it may enter the same grid box several times (Ho et al. 2005). The TC genesis frequency is calculated in the same way. In this study, TCs that influence Taiwan are defined as those which pass through the area of 21–26N, 119–125E (box in the embedded map of Fig. 1; Chu et al. 2007).

To analyze the environmental steering effect on TC movement, we simply calculated the deep-layer mean flow (DLMF; V_{trop}) as

$$V_{\text{trop}} = \frac{1}{P_b - P_t}\int_{p_t}^{p_b} V\,dp \tag{1}$$

where P_b and P_t are fixed at the 850 and 200 hPa levels, respectively. Velden and Leslie (1991) indicated that the initialization of a barotropic TC track forecast model with a variable-depth wind analysis that best approximates the environmental steering can significantly reduce the mean forecast error relative to a "fixed-depth" analysis. However, the DLMF defined above still provides the overall best forecast of TC tracks.

The forecast performance of the statistical model developed in this study is measured by its mean absolute error (MAE):

$$\text{MAE} = \frac{1}{N}\sum_{i=1}^{N} |O_i - f_i| \tag{2}$$

where N, O_i, and f_i are the number of samples, observed and forecast values, respectively. In this study, the of Student's t test is used for statistical significance test. More details can be found in the reference book of Wilks (1995).

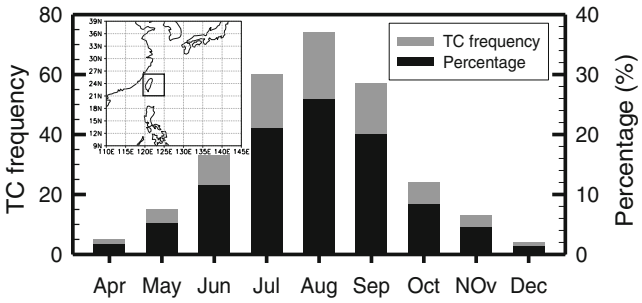

Fig. 1 The frequency of TCs that influence Taiwan and the percentage of TC frequency in each month to total TC frequency for July to September (JAS) during the period of 1951–2011 (61 years)

3 Development of the multiple linear regression model

3.1 Predictors associated with large-scale environments

We first examine how monthly frequencies of TCs influencing Taiwan are distributed (Fig. 1). A total of 294 TCs influenced Taiwan during the analysis period of 61 years, namely, on average 5 TCs influenced Taiwan per year. The frequency of over 40 TCs occurred in the 3 months of July (62), August (79), and September (59) (hereafter JAS), each representing about 20–30 % of the annual frequency, and totally accounting for approximately 70 % of the annual frequency. This indicates that climatologically more than three fifths of TCs that influence Taiwan in a year occur in JAS. Therefore, in this study, we focus on TCs influencing Taiwan during JAS and define these 3 months as boreal summer. We also divide the entire analysis period of the 61 years into two periods: the calibration period 1951–2000 (50 years) for the development of the statistical model and the validation period 2001–2011 (11 years) for verifying the prediction performance of the statistical model developed.

To identify potential predictors for the multiple linear regression model, a lag-correlation analysis between the boreal summer TC frequency around Taiwan and the large-scale environments (variables of horizontal wind and SST) in the preceding winter (December–February) and spring (March–May) is conducted for the calibration period (Fig. 2). With regard to the large-scale environments here, observed values, not anomalies, are used to obtain promptly predicted values from the statistical model. High correlation coefficients of over ±0.4 at the 99 % confidence level are found mainly in February and May. Although somewhat high correlations exist in other months in other regions (not shown), the large-scale environments in regions (for example, the Arctic and the Antarctic, Europe, Africa, west Asia, etc.) not too far away from Taiwan are selected so that the variation of TC frequency can be easily explained. The high correlations are found in the upper troposphere (200 hPa level), middle troposphere (500 hPa level), and lower troposphere (850 hPa level) in February, as well as in the middle troposphere and in SST in May.

In the lower troposphere in February, high negative and high positive correlations with meridional wind are shown over Australia and the northeastern sea of Australia, respectively (Fig. 2a). This indicates that if the lower tropospheric anticyclonic circulation to the east of Australia is strengthened in February, more TCs will influence Taiwan in the coming summer. In the middle troposphere in the same month, high positive and high negative correlations with meridional wind are found to the south and the east of the Philippines, respectively (Fig. 2b). This implies that when the middle tropospheric anticyclonic circulation is intensified in the WNP in February, TC frequency around Taiwan

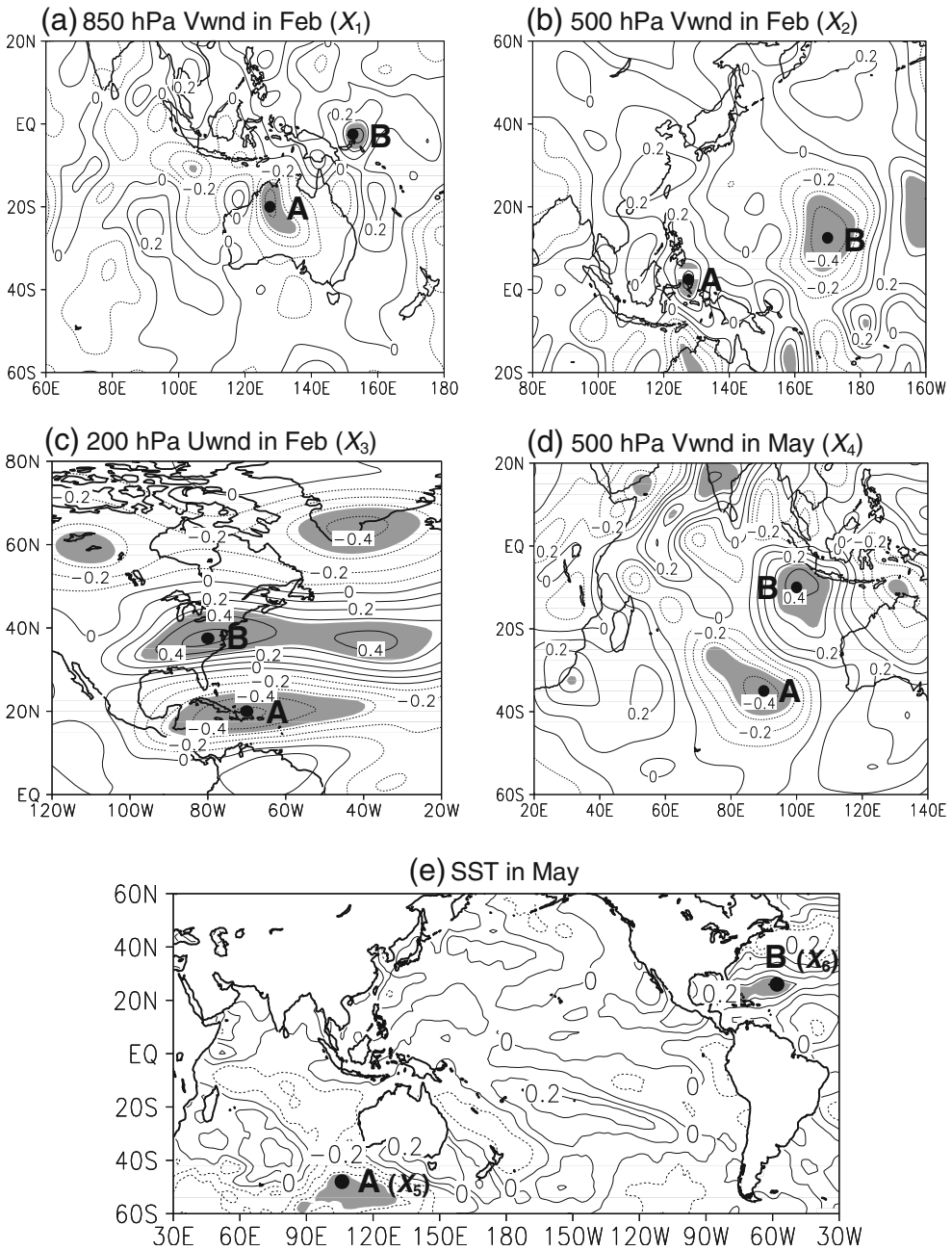

Fig. 2 Correlation distributions of the frequency of TCs that influence Taiwan for JAS and **a** meridional wind at 850 hPa in February, **b** meridional wind at 500 hPa in February, **c** zonal wind at 200 hPa in February, **d** meridional wind at 500 hPa in May, and **e** sea surface temperature (SST) in May. The contour interval is 0.1. *Shaded areas* are significant at the 99 % confidence level. *Points* denote the highest correlation coefficient locations in each variable

in summer increases. It is considered that southerly along the western periphery of the strengthened western North Pacific high may persist until the coming summer and steers TCs toward the Taiwan area. In the upper troposphere, in the same month, high positive correlation and high negative correlations with zonal wind are shown over Northeast America and around the Caribbean Sea, respectively (Fig. 2c). This means that when the upper tropospheric anticyclonic circulation in February is intensified to the east of North America, TC frequency around Taiwan increases in the coming summer.

In May, high negative and high positive correlations with middle tropospheric meridional winds are found in the southwest of Australia and the northwest of Australia, respectively (Fig. 2d). This indicates that if the middle tropospheric anticyclonic circulation to the west of Australia in May is intensified, TC frequency around Taiwan would increase in summer. In short, when the anticyclonic circulation is intensified in February and May in the four regions mentioned above, TC frequency around Taiwan will increase in the coming summer. In May, high negative and high positive correlations are shown to the southwest of Australia and the southeastern sea of North America, respectively (Fig. 2e), indicating the remote effect of ocean thermal conditions on TC activity around Taiwan.

3.2 Multiple linear regression model

We now turn to analyze time series of the values extracted at the high correlation points for every predictor presented above (Fig. 3). For the atmospheric circulation predictors, the difference in values between the positive and negative correlation points is calculated instead of the area mean. It is considered that the higher the values calculated with this method, the more significantly the anticyclonic circulation (even though it is not closed circulation) intensifies in each of the four regions. As a result, the values higher than the correlation coefficient at each correlation point analyzed above are calculated for all predictors. All the correlation coefficients are significant at the 99 % confidence level. However, such high correlation coefficients may change when the trends in time series are removed from the variation of independent variables (predictors) and dependent variable (TC frequency around Taiwan). Therefore, we repeat the analysis of the correlation between the two variables after the trends of each predictor and the TC frequency around Taiwan is removed. However, the correlation coefficients after and before the removal do not differ significantly and are still significant at the 99 % confidence level. Therefore, we can construct a multiple linear regression model (hereafter, MLRM) to predict the frequency of TCs influencing Taiwan in boreal summer using the six large-scale environmental predictors as follows:

$$\mathrm{MLRM} = 0.21x_1 + 0.21x_2 + 0.03x_3 + 0.07x_4 - 1.02x_5 + 0.43x_6 - 0.16 \quad (3)$$

where, x_1 ,x_2,x_3, and x_4 represent the differences in 850, 500, 200 hPa winds in February and 500 hPa wind in May, respectively, between the high positive correlation points and the high negative correlation points (Figs. 2a–d); and x_5 and x_6 are SSTs at A and B points in May, respectively (Fig. 2e). In fact, in this study, we use predictors to explain the variation of TC frequency around Taiwan through analyzing the large-scale atmospheric circulations nearby. This is also the reason why statistical methods, such as the stepwise multiple regression, are not used to select the optimum predictors. Moreover, if predictors are screened by statistical methods, it may be difficult to explain the relationships between the TC frequency around Taiwan and the predictors.

Figure 3 shows the hindcast of the summer TC frequency around Taiwan with this MLRM during the calibration period. The hindcast reproduced the observed interannual and interdecadal variations of TCs (MAE=0.5, r=0.88 at the 99 % confidence level; lowest panel in Fig. 3). In particular, the MLRM performs well for the hindcast of TC frequencies in the two extreme years with six TCs and one TC, respectively. Moreover, TC frequency hindcasted by this MLRM during the validation period corresponds relatively well to the observed TC frequency with the MAE of 0.72 (Fig. 4).

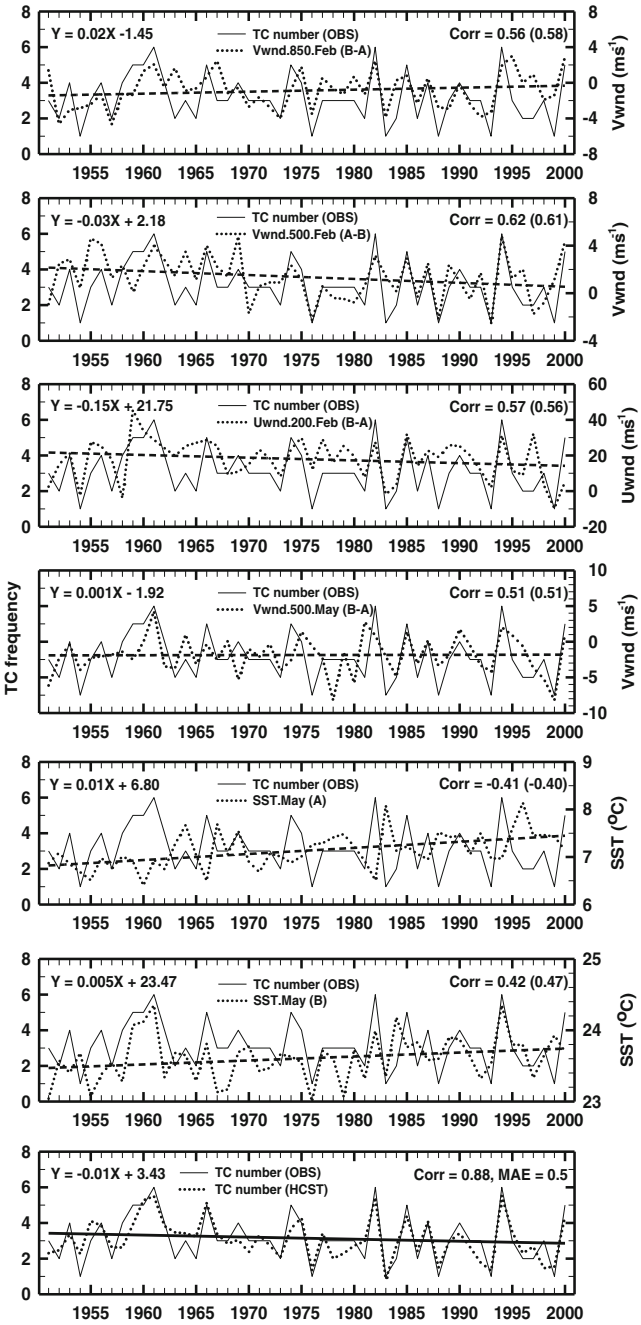

Fig. 3 Time series of the TC frequency (*solid line*) in Taiwan in JAS and the predictor (*dotted line*) at the highest correlation point among the correlation distributions of each predictor in Fig. 2 during the calibration period (1951–2000). The last panel denotes time series of the observed TC frequency (*solid line*) and TC frequency (*dotted line*) hindcasted by the multiple linear regression model (MLRM) developed using six predictors during the calibration period. *Bold dashed and solid lines* represent trends (formula in the *uppermost of the left side*) of six predictors and TC frequency in Taiwan, respectively

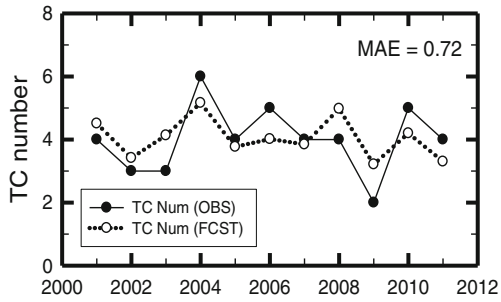

Fig. 4 Time series during the validation period (2001–2011) for the observed (*solid line with a closed circle*) and hindcasted (*dotted line with an open circle*) TC frequencies in Taiwan by the MLRM

4 Verification of the MLRM

In this section, the following two analyses are carried out to verify the MLRM : (1) statistical cross-validation (CV) test and (2) contrasting analysis for the large-scale environments between the high and low TC frequency years in the 61 years hindcasted by the MLRM.

4.1 Cross-validation analysis

To examine the temporal stability of the regression coefficients, statistical CV tests for the statistical model are commonly performed (Wilks 1995). This study also validates the MLRM through statistical CV tests.

To hindcast the TC frequency during the calibration period at 10-year intervals, a multiple linear regression model is developed using six predictors from the other 40 years. After this process is repeated, a total of five multiple linear regression models (hereafter, CV models) are constructed during the calibration period. These five CV models are also used to hindcast TC frequency around Taiwan during the validation period. In other words, each of the five CV models hindcasts TC frequency for 21 years in total (10 years of the calibration period plus 11 years of the validation period). The time series of TC frequencies observed (solid line) and hindcasted by the CV model (dotted line) and the MLRM (dashed line) are presented in Fig. 5. It is seen that the CV models hindcast reasonably well not only the TC frequency of every 10 years during the calibration period but also the TC frequency during the validation period in all time series. In addition, the TC frequencies hindcasted by these five CV models are very similar to those hindcasted by the MLRM (five correlation coefficients are over 0.95, which are significant at the 99 % confidence level). Such a high correlation is a result of almost no difference in regression coefficients between the MLRM and the five CV models (Table 1). Therefore, the above statistical CV test results demonstrate that the MLRM developed in this study is a valid and stable tool for seasonal prediction of TCs affecting Taiwan in boreal summer.

4.2 Difference between high and low TC frequency years hindcasted by the MLRM

To further verify the validity of the MLRM developed in this study, we select 12 years with the highest TC frequencies around Taiwan (hereafter, positive years) and 12 years with the lowest TC frequencies (hereafter, negative years) hindcasted by the MLRM in the 61 years, and analyze the mean differences between the two groups in terms of the large-scale environments. To reduce the effects of ENSO on the large-scale environments and TC activity in the average of JAS, each 12 years are selected from the remaining years (neutral ENSO years) except for the El Niño years (1951, 1953, 1957, 1963, 1965, 1972, 1982, 1987, 1991, 1997, 2002, 2004, 2009) and the La Niña years (1954–1956, 1964, 1970–1971, 1973, 1975, 1988, 1998, 2007, 2010), even though in February and May in the entire analysis period of 61 years, the TC frequency around Taiwan in JAS has low correlations with the Niño-3.4 indices, with correlation coefficients of −0.08 and 0.07, respectively. So two thirds of the whole data sets, except for El Niño or La Niña years (total 25 years), were chosen for the analysis below.

The two sets of 12 years selected are shown in Table 2. In the positive years, no year that the MLRM hindcasts shows a TC frequency of less than four TCs and the same result is found in the negative years except for 1958. There is almost no difference in the average TC frequencies hindcasted by the MLRM and that observed between the positive and negative years. In particular, in both hindcast and observation, the average TC frequency in the positive years is about twice of that in the negative years. In addition, the total genesis frequency of TCs in JAS in the positive years is also much higher than in the negative years in the subtropical WNP (SWNP; positive years, 195; negative years, 166). The difference in the total genesis frequency of TCs in JAS between the two groups is significant at the 90 % confidence level.

4.2.1 Large-scale environments

To examine the characteristics of large-scale atmospheric circulations in the two groups classified above, the difference in the DLMF in February, May, and JAS between the two groups is analyzed (Fig. 6). In February, the anomalous anticyclones are centered in the eastern inland region of Australia and the South Indian Ocean (upper panel in Fig. 6a). The flow from the anomalous anticyclone centered in the South Indian Ocean is connected to the anomalous anticyclone over Australia. This connected flow is joined by the easterly around the equator from the anomalous anticyclone located in the subtropical western North Pacific, and the two flows together form the equatorial trade easterly. This trade wind turns into a southerly around 120°E before

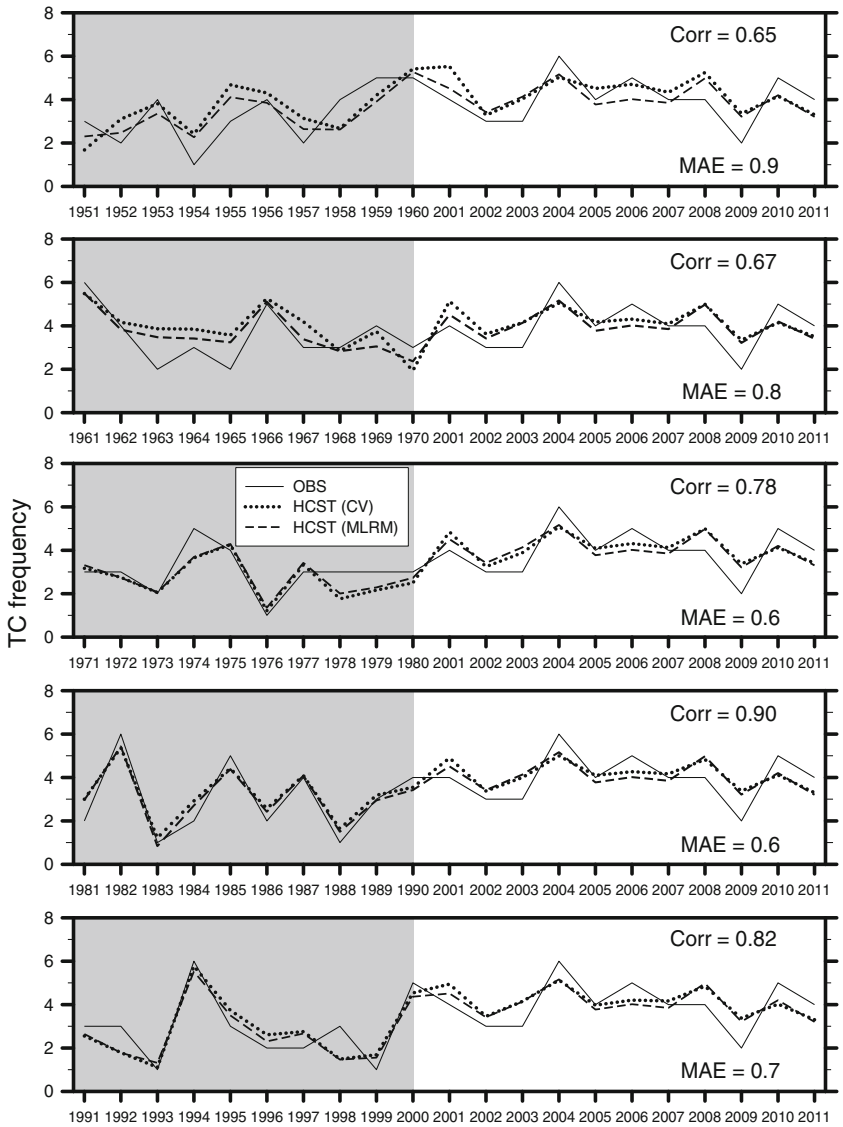

Fig. 5 Time series of the TC frequencies in Taiwan that are observed (*solid line*) and hindcasted by the CV model (*dotted line*) and MLRM (*dashed line*). The correlation coefficient and MAE are calculated between TC frequencies that are observed and hindcasted by the CV model

reaching Taiwan. On the other hand, in the North Pacific, the huge anomalous anticyclone is centered to the south of the Aleutian Islands, and the ridge of this anticyclone extends southwestward to the subtropical western North Pacific (lower panel in Fig. 6a). The southerly associated with the ridge is predominant along the coastal region of East Asia. This indicates that the favorable environment for the potential high TC frequency in boreal summer in the coastal regions of East Asia, including Taiwan, is already established in February. The flow from the huge anomalous anticyclone centered to the south of the Aleutian Islands is connected to the anomalous anticyclone centered in the

Table 1 Regression coefficients and constants in the MLRM and multiple linear regression models developed through the statistical CV test for hindcasting of TC frequency in Taiwan in each decade during the calibration period

Model		Regression coefficient of predictors						Const
		x_1	x_2	x_3	x_4	x_5	x_6	
MLRM		0.21	0.21	0.03	0.07	−1.02	0.43	−0.16
Cross-validation (CV) model	1950s	0.10	0.32	0.03	0.05	−1.01	0.67	−6.29
	1960s	0.25	0.30	0.04	0.01	−0.63	0.15	3.20
	1970s	0.19	0.25	0.03	0.10	−0.89	0.57	−4.44
	1980s	0.18	0.23	0.02	0.07	−0.84	0.62	−5.98
	1990s	0.24	0.24	0.03	0.06	−0.78	0.56	−5.14

Table 2 The highest 12 years and the lowest 12 years hindcasted by the MLRM in terms of TC frequency around Taiwan excluding El Niño and La Niña years in JAS for 1951–2011

Positive years			Negative years		
Year	OBS	HCST	Year	OBS	HCST
1959	3.9	5	1952	2.5	2
1960	5.3	5	1958	2.6	4
1961	5.5	6	1976	1.4	1
1962	3.8	4	1978	2.0	3
1966	5.1	5	1979	2.3	3
1985	4.4	5	1980	2.7	3
1994	5.5	6	1983	0.8	1
2000	4.4	5	1984	2.7	2
2001	4.7	4	1986	2.4	2
2005	3.9	4	1992	1.8	3
2006	4.2	5	1993	1.3	1
2008	4.7	4	1996	2.3	2
AVG	4.6	4.8	AVG	2.1	2.3
STD	0.6	0.7	STD	0.6	1.0

OBS observed Taiwan TC frequency, *HCST* hindcasted Taiwan TC frequency, *AVG* average, *STD* standard deviation

eastern coastal region of North America through the form of trade wind around 130°W. The anomalous cyclone is located between these two anticyclones (intermountain region of North America). This spatial distribution of anomalous pressure systems in the North Pacific and North America is similar to the negative Pacific/North American (PNA) teleconnection pattern (hereafter, PNA pattern; Wallace and Gutzler 1981).

In May, although the anomalous pressure systems in February weaken, they still persist (Fig. 6b). The flows from these two anomalous anticyclones centered in the northwest and the northeast of Australia still form part of the trade winds (upper panel in Fig. 6b). Particularly, the trade winds from the anomalous anticyclone centered in the northeastern sea of Australia shift northwestward to the south of Taiwan. Anomalous anticyclones are still centered in the eastern sea of Japan, the southeastern sea of the Aleutian Islands, and the eastern inland region of North America (lower panel in Fig. 6b). In particular, the coastal region of East Asia is still under the influence of the southerly related to the anomalous anticyclone centered in the eastern sea of Japan with the anomalous cyclone over northeastern China. Therefore, it is considered that the environment that influences TC activity around Taiwan is established well before the TC season. As stated above, the anomalous anticyclones intensify in all of the four regions where high correlations exist in both February and May, and all of them are related to the increase of TC frequency around Taiwan in the coming summer.

It is shown that the anomalous anticyclones intensify over the seas west and east of Australia in JAS, namely in the austral winter (upper in Fig. 6c). The flows from these two anomalous anticyclones still contribute to form the trade winds with the anomalous anticyclone in the subtropical western North Pacific. Especially, the trade wind that formed by the anomalous anticyclone over the eastern sea of Australia moves to the Taiwan area along the monsoon trough between 120° and 140°E. The two anomalous anticyclones around Australia are referred to as the typical pattern of anomalous pressure systems in the positive phase of the Antarctic Oscillation (AAO; Gong and Wang 1999;

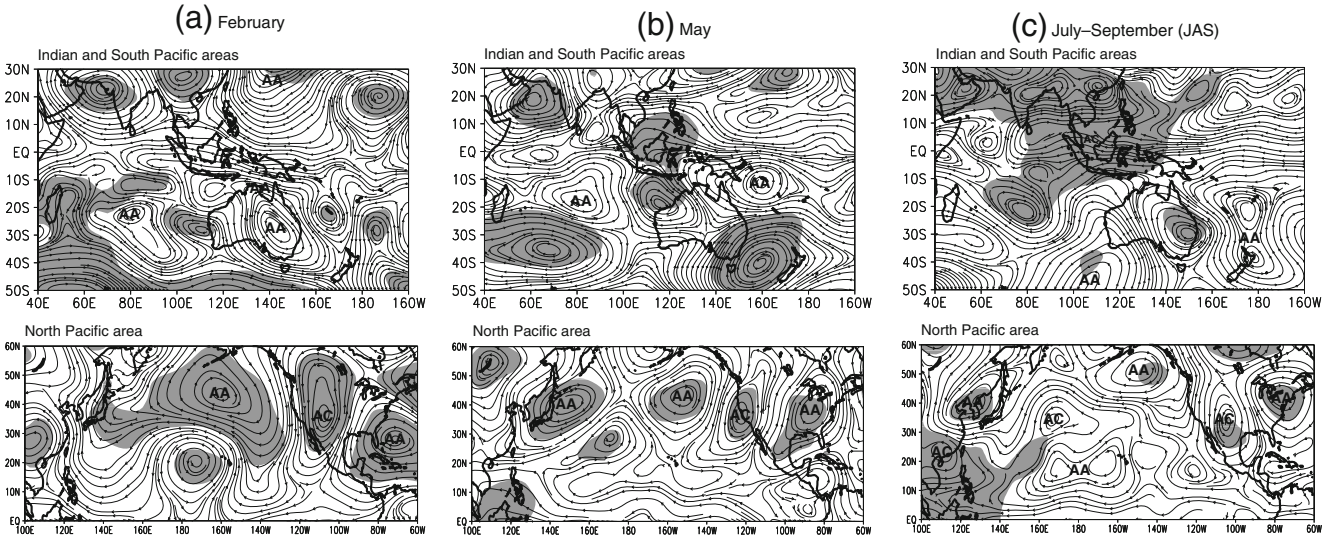

Fig. 6 Difference in the DLMFs between positive years and negative years over Indian and South Pacific areas (*upper panel*) and North Pacific area (*lower panel*) **a** in the preceding February, **b** in the preceding May, and **c** in the current JAS. *Shaded areas* are significant at the 95 % confidence level. *AA* anomalous anticyclone, *AC* anomalous cyclone

Thompson and Wallace 2000). The anomalous anticyclone centered over the sea west of Australia is called the Mascarene high (Xue et al. 2004), even though its location is somewhat different from that defined in Xue et al. (2004), and has already been analyzed previously as one of the main factors influencing the Indian summer monsoon (e.g., Ramaswamy and Pareek 1978; Rodwell 1997). The anomalous anticyclone (Australian high; Ho et al. 2005) in the South Pacific Ocean intensifies the cross-equatorial flow in the western equatorial Pacific. The intensified cross-equatorial flow modulates the Intertropical Convergence Zone in the subtropical western North Pacific and western North Pacific high, both affecting TC activity in the western North Pacific. Ho et al. (2005) studied in detail the change in TC activity over the western North Pacific by AAO, and Choi et al. (2010) showed that AAO is one of the potential predictors of a statistical model for predicting the seasonal TC genesis frequency in the subtropical western North Pacific. On the other hand, the negative PNA pattern, which has intensified in February, weakens during JAS (lower in Fig. 6c). Most of the previous studies related to the PNA and AAO teleconnection patterns have emphasized the simultaneous climatic influence in cold seasons when these patterns are in their most active phase. However, it should be noted that the teleconnection patterns during cold seasons including PNA and AAO also account for a large portion of the total variance in the large-scale atmospheric circulation during warm seasons (Northern Hemisphere: May–October, Southern Hemisphere: November–April) (Rogers 1990; Thompson and Wallace 2000). In addition, many climate systems significantly influenced by the cold season teleconnection patterns can have long memory and can feed back to the atmospheric circulations with time lags (Gong and Ho 2003). To examine if PNA and AAO teleconnection patterns are observed in seasons other than the cold season in both hemispheres, we conduct an empirical orthogonal function analysis for 700 hPa geopotential height in February, May, and JAS in the region north of 20°N (for PNA) and the region south of 20°S (for AAO; Fig. 7). Generally, the PNA (AAO) teleconnection pattern is referred to as the second (first) leading mode from the EOF analysis of monthly mean height anomalies at 1,000 or 700 hPa in the Northern Hemisphere (Southern Hemisphere). It is seen that the two teleconnection patterns are the most intense in their corresponding winter season (Northern Hemisphere: February, Southern Hemisphere: JAS), and also exist in the other two seasons. In addition, the principal components in this study are consistent with the AAO and PNA indices provided by NOAA/Climate Prediction Center in February, May, and JAS, respectively (Table 3). All the correlation coefficients shown in Table 3 are significant at the 99 % confidence level.

On the other hand, the anomalous anticyclonic circulation forms in the region from the Aleutian Islands to the coastal region of East Asia, while the anomalous anticyclone still

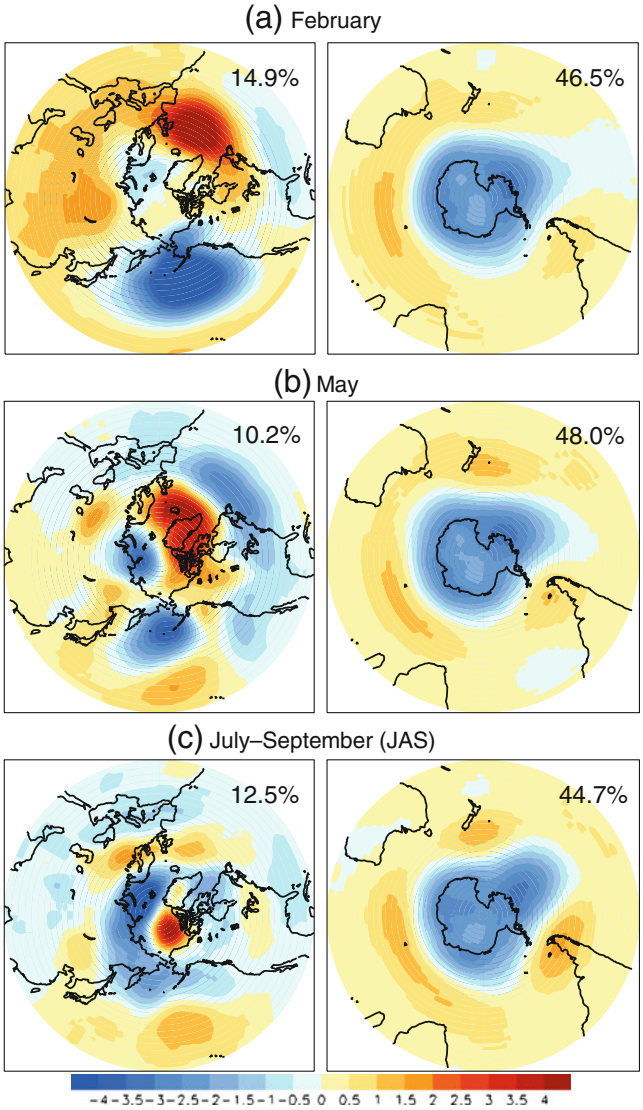

Fig. 7 Regression maps of the second (*left panel*) and the first (*right panel*) EOFs on 700 hPa geopotential height in **a** February, **b** May, and **c** JAS in the region north of 20°N (*left panel*) and 20°S (*right panel*) during the period 1979–2011. Eigenvectors are multiplied by 100

remains in the east coastal regions of North America (lower panel in Fig. 6c). Here, Taiwan is influenced by the flows converged between the southeasterly from the monsoon

Table 3 Correlation coefficients between principal components (PCs) in this study and AAO and PNA indices provided by NOAA/Climate Prediction Center (CPC) in February, May, and JAS, respectively

	Correlation coefficients	
	AAO	PNA
February	0.96	0.83
May	0.97	0.71
July–September	0.95	0.73

trough centered in southern China and the easterly from the anomalous anticyclone centered in Korea. This spatial distribution of anomalous pressure systems around Taiwan represents a pattern exactly opposite to the spatial distribution of anomalous pressure systems in the below-normal TC frequency years around Taiwan found by Chu et al. (2007). Therefore, it shows that these flows converging around Taiwan play an important role in steering TCs formed in the western North Pacific toward Taiwan region.

In short, the results of the large-scale atmospheric circulation analyzed above indicate that the positive AAO pattern and the negative PNA pattern intensify the trade winds in the equatorial Pacific. The intensified trade winds, in turn, play an important role in steering TCs toward Taiwan area. This implies that the four large-scale atmospheric circulation predictors influence TC frequency around Taiwan not by themselves, but by interaction among the predictors. This is consistent with high correlations among predictors shown in Table 4.

On the other hand, anomalous warm SST appears in the period from February to JAS in most regions except in the southeast of western North Pacific (Fig. 8). As warm SST is one of the favorable environmental conditions for TC genesis and development, it can lead to more TC geneses during JAS in the positive years, as stated above. Also, the spatial distributions of anomalous SST in the sea southwest of Australia (40°S, 60°–120°E) and the sea east of North America seem to be related to the anomalous anticyclonic circulation in these regions, as analyzed above. This is demonstrated by the relatively high correlations (r=−0.32 at the 95 % confidence level) between predictors x_5 and x_4 and (r=0.35 at the 95 % confidence level) between predictors x_6 and x_3 during the analysis period of the 61 years (Table 4). Here, the predictor x_3 is the zonal wind in February and x_6 is SST in May. Therefore, it is considered that atmospheric circulation predictor (x_3) feeds back to the SST predictor (x_6) with time lags as stated above.

The difference in large-scale environments between the two groups indicates that the positive AAO pattern and the negative PNA pattern intensified since February may be related to the increase of TC frequency around Taiwan during the boreal summer. Therefore, to examine the relationships between the six large-scale environmental predictors (including TC frequency) and the two teleconnection patterns, we analyzed the correlation between the six predictors in February, May, and JAS (including TC frequency in JAS) and the AAO and PNA indices in the same months (Table 5). The data from 1979 to 2011 (for 33 years) provided by National Oceanic and Atmospheric Administration/Climate Prediction Center were used for the indices of the two teleconnection patterns. The TC frequency in JAS is related to the AAO pattern in February and the boreal summer at the 90 % confidence level, while it shows higher negative correlation with PNA pattern in May at the 95 % confidence level. However, the TC frequency does not have high correlation with the two indices in any month at the 99 % confidence level. The negative correlation of TC frequency with the PNA pattern may be associated with the fact that the

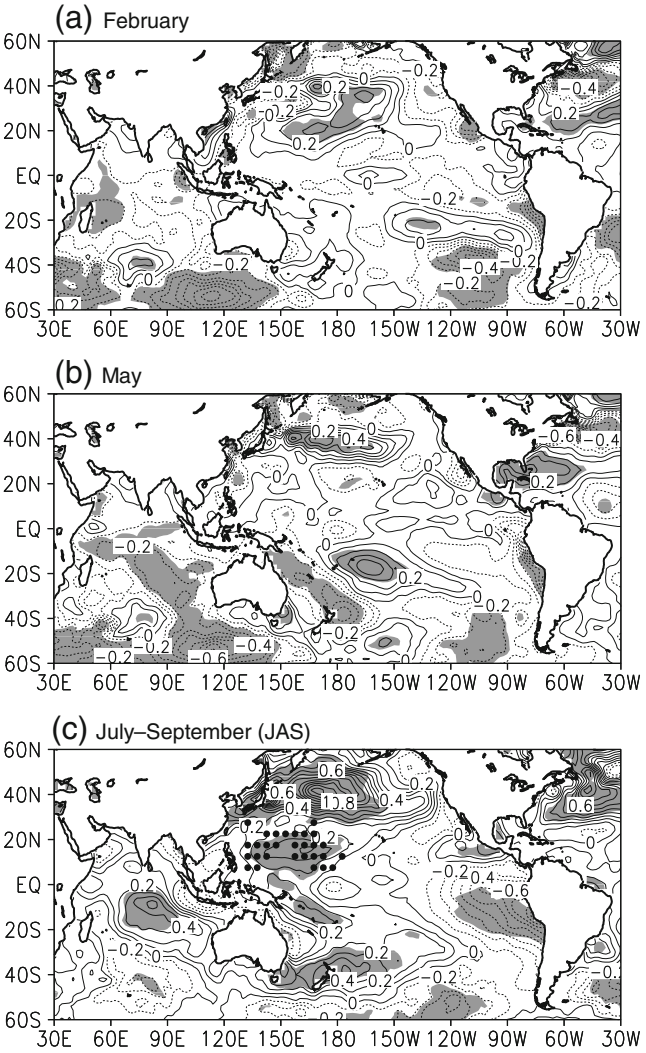

Fig. 8 Same as Fig. 6, but for SST. In **c**, *dots* denote the main TC genesis locations for the positive years. *Shaded areas* are significant at the 95 % confidence level. The contour interval is 0.1 °C

Table 4 Cross-correlation coefficients among various predictors during the period 1951–2011 (61 years)

Predictors	x_1	x_2	x_3	x_4	x_5	x_6
x_1	1.00	0.35	0.42	0.37	−0.11	0.41
x_2	0.35	1.00	0.34	0.52	−0.28	0.37
x_3	0.42	0.34	1.00	0.49	−0.33	0.35
x_4	0.37	0.52	0.49	1.00	−0.32	0.32
x_5	−0.11	−0.28	−0.33	−0.32	1.00	−0.16
x_6	0.41	0.37	0.35	0.32	−0.16	1.00

Figures in dark, middle, and light gray shadings are significant at the 99, 95, and 90 % confidence levels, respectively

Table 5 Correlation coefficients between TC frequency affecting Taiwan and predictors, as well as between TC frequency affecting Taiwan and climate indices (AAO and PNA) during the period 1979–2011 (33 years)

Figures in dark, middle, and light gray shadings are significant at the 99, 95, and 90 % confidence levels, respectively

Climate index		Taiwan TC frequency	Predictors					
			x_1	x_2	x_3	x_4	x_5	x_6
AAO	February	0.33	0.43	0.50	0.27	0.42	−0.35	0.31
	May	0.16	0.31	0.27	0.31	0.33	−0.29	0.22
	JAS	0.28	0.37	0.25	0.38	0.30	−0.22	0.24
PNA	February	−0.29	−0.45	−0.44	−0.70	−0.43	0.25	−0.30
	May	−0.41	−0.46	−0.52	−0.49	−0.57	0.35	−0.55
	JAS	−0.21	−0.33	−0.24	−0.41	−0.23	0.24	−0.21

spatial distribution of the differences in the large-scale atmospheric circulation between the two groups is negatively correlated to the PNA pattern, as analyzed above. On the other hand, there are high correlations between the two indices and the six predictors. AAO pattern shows relatively high correlations with the six predictors in February and in JAS.

As the AAO is the teleconnection pattern in the Southern Hemisphere, it shows the correlations with atmospheric circulations in the east (predictor x_1) and the west (predictor x_4) of Australia in all months at the confidence level of 90 % or higher. Especially, it shows high correlation with atmospheric circulation (predictor x_2) in the subtropical western North Pacific in February at the 99 % confidence level. As analyzed above, this is because the anomalous anticyclonic circulation in the Pacific Ocean of the Southern Hemisphere is connected directly to the atmospheric circulation in the Pacific Ocean of the Northern Hemisphere through the trade winds in the positive AAO phase. The correlation with the atmospheric circulation (predictor x_3) around the sea east of North America is not low during JAS. The variation of SST (predictor x_5) in the sea west of Australia is also correlated with the AAO pattern in February at the 95 % confidence level. The PNA pattern shows higher correlations with the six predictors than with the AAO pattern. In particular, high correlations over 95 % confidence level are concentrated mostly in February and May. As the PNA is a teleconnection pattern in the boreal winter, the highest correlation with the atmospheric circulation is found in February around the eastern sea of North America (predictor x_3). Also, the PNA pattern shows high correlations with all atmospheric circulation predictors (x_1 to x_4) and the SST predictor (x_6) at the 99 % confidence level in May. Therefore, the above correlation analysis indicates that the variation of large-scale atmospheric circulation around Taiwan associated with the variation of the two teleconnection patterns influences the frequency of TCs that affect Taiwan in boreal summer.

4.2.2 TC activity

As analyzed above, the difference in the large-scale environments between the two groups can influence TC activity in the western North Pacific. Therefore, here we analyze the difference in TC genesis frequency and TC passage frequency in JAS between the two groups (Fig. 9).

The main TC genesis regions of the two groups are clearly separated (Fig. 9a). TCs in the positive years occur mainly in the northwestern region of the western North

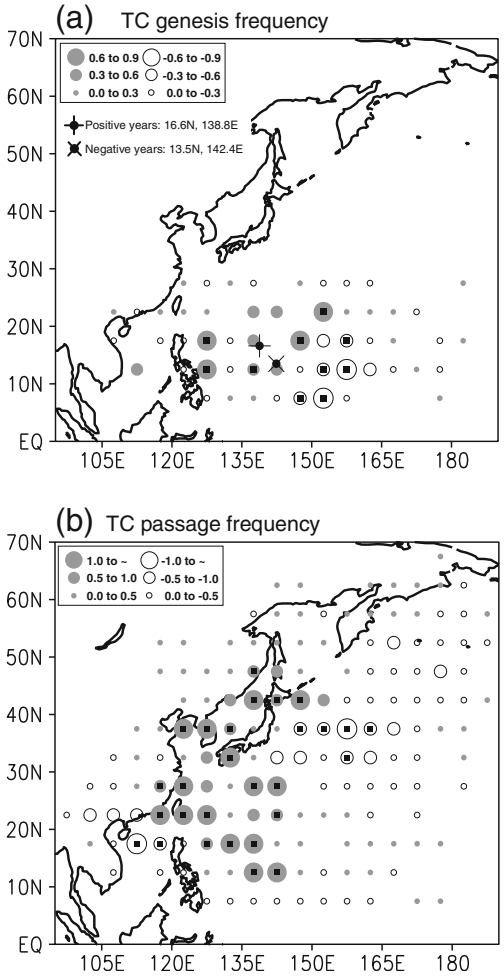

Fig. 9 Differences in the **a** TC genesis frequency and **b** TC passage frequency between the highest 12 years (positive years) and the lowest 12 years (negative years) hindcasted by the MLRM on the TC frequency in Taiwan for 1951–2011. *Small squares inside circles* are significant at the 95 % confidence level

Pacific, and those in the negative years occur mainly in the southeastern region of the western North Pacific. This feature is clearly seen from the average TC genesis locations of the two groups (positive years: 16.6°N, 138.8°E; negative years: 13.5°N, 142.4°E). Here, the latitude and longitude differences in TC genesis locations between the two groups are significant at the 99 % confidence level and at the 95 % confidence level, respectively. This difference in TC genesis locations between the two groups can be explained by the difference in DLMF between the two groups during JAS (lower panel in Fig. 6c). The anomalous anticyclonic circulation and the anomalous cyclonic circulation intensify in the southeast of and the northwest of 25°N in the subtropical western North Pacific, respectively. This pattern of pressure system, namely High in South/Low in North in the subtropical western North Pacific, offers a favorable environment for TC genesis in the more northwestern region of the subtropical western North Pacific in the positive years.

The cause of the difference in TC genesis locations between the two groups can be found not only in the difference in the large-scale atmospheric environments but also in the difference in the SST distributions (Fig. 8). As analyzed above, the warm SST anomaly intensifies in most regions except in the southeastern region of the subtropical western North Pacific from February to JAS in the positive years. In other words, there is also an SST pattern of Low in South/High in North in the subtropical western North Pacific. This spatial distribution of SST can also contribute to a favorable environment for TC genesis in the more northwestern region of the subtropical western North Pacific in the positive years. This is true since the main TC genesis location in the positive years is generally identical to the warm SST region in the subtropical western North Pacific (dots in Fig. 8c). In general, as the convection moves to the west in the subtropical Pacific in La Niña phase, TCs tend to occur more in the northwestern region of the subtropical western North Pacific (Wang and Chan 2002; Elsner and Liu 2003; Chen et al. 2006). This implies that difference in the spatial distribution of TC genesis locations between the two groups is similar to the characteristic of the La Niña phase, despite the removal of ENSO effects in this study, which might indicate the influence of climate factors (such as AAO and PNA in this study) other than ENSO events (Chu et al. 2007).

Regional differences between the two groups during JAS are clear in TC passage frequency as well (Fig. 9b). In the positive years, TCs move northwestward mainly from the sea east of the Philippines to Taiwan or northwestward from the sea southeast of Japan to Korea and then northeastward to the north of Japan. However, in the negative years, TCs tend to move northwestward from the Philippines to southern China or mainly in the western North Pacific far away from the coasts of East Asia. In other words, TC passage frequency in the coastal countries of East Asia is higher in the positive years than in the negative years. This regional difference in TC passage frequency between the two groups can be explained also by the difference in DLMF between the two groups during JAS (lower panel in Fig. 6c). The southeasterly from the anomalous cyclone centered in south China moves toward Taiwan and the easterly from the anomalous anticyclone centered in Korea moves toward the central coast of China. As indicated above, these two flows play a decisive role in steering TCs to affect Taiwan in the positive years, while also obstructing TCs to move to the coastal countries of East Asia in the negative years. Ho et al. (2005) also showed the high frequency of TCs that influence the coastal regions of East Asia due to the anomalous anticyclone intensified in inland of the mid-latitudes of East Asia in the positive AAO phase.

5 Summary

In this study, we have developed a statistical model (MLRM) to predict the frequency of TCs that influence Taiwan during boreal summer (JAS) by using the large-scale environmental predictors in February and May. The entire analysis period of 61 years is classified into the 50-year calibration period (1951–2000) for the development of the MLRM and the 11-year validation period (2001–2011) for the verification of the developed MLRM. Large-scale environmental predictors are selected at points with high correlations at the 99 % confidence level through the lag-correlation analysis with horizontal winds in upper, middle, and lower troposphere in the preceding winter and spring. The high correlations with the atmospheric circulations and SST conditions in six regions can be summarized as follows: four large-scale atmospheric circulation predictors are (1) anomalous anticyclone in the east of Australia, (2) anomalous anticyclone in the sea west of Australia, (3) anomalous

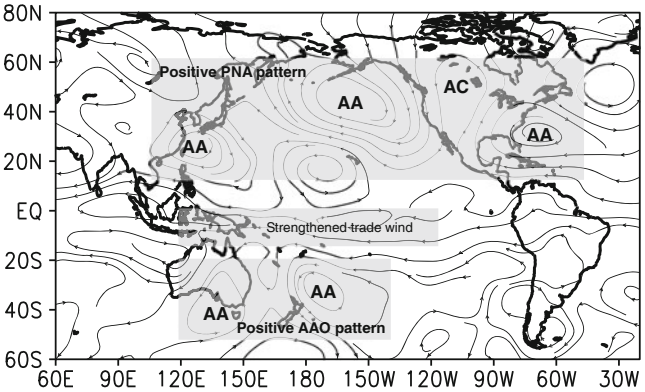

Fig. 10 Schematic illustration of atmospheric changes during the high TC frequency years around Taiwan in JAS. *AA* anomalous anticyclone, *AC* anomalous cyclone

anticyclone in the subtropical western North Pacific, (4) anomalous anticyclone around the sea east of North America, and two SST predictors are (5) cold SST in the southwest of Australia, (6) warm SST in the sea southeast of North America. The MLRM using these six large-scale environmental predictors hindcasts considerably well the observed TC frequency in both the calibration period (r=0.88 at the 99 % confidence level) and the validation period.

The validity of the MLRM developed in this study is verified both based on statistical cross-validation (CV) tests and by contrasting analysis of differences between high and low TC frequency years hindcasted by the MLRM in both the large-scale environments and TC activity. In the statistical CV tests, the results show little differences between TC frequencies hindcasted by the five models from the statistical CV test and hindcasted by the MLRM. The regression coefficients of the six predictors consisting of the five models from the statistical CV test are also similar to those of the MLRM. Analysis of the difference in the large-scale environments between high and low TC frequency years indicates that the six predictors are related to two teleconnection patterns in the Southern Hemisphere and the Northern Hemisphere. The anomalous anticyclones in the east and the west of Australia are related to the positive AAO pattern, and the anomalous anticyclones in the subtropical western North Pacific and around the eastern sea of North America are related to the negative PNA pattern. These two teleconnection patterns (AAO and PNA patterns) persist from February through JAS. Also, SSTs to the southwest of Australia and in the western North Atlantic represent the spatial distributions of the anomalous atmospheric circulations associated with the positive AAO pattern and the negative PNA pattern, respectively. These characteristics are shown through the correlation analysis between the six predictors and the indices of the two teleconnection patterns. Therefore, the MLRM developed in this study reflects the mechanism by which the anomalous anticyclone around Australia (positive AAO pattern) and anomalous anticyclone from the eastern sea of North America, through the Aleutian Islands, to the subtropical western North Pacific (negative PNA pattern) are strengthened since February. Consequently, the trade wind intensifies in the equatorial and tropical Pacific and plays a decisive role in steering TCs to affect Taiwan. The schematic illustration about this mechanism is shown in Fig. 10.

On the other hand, the southerly intensifies in the coastal region of East Asia in the high TC frequency years (positive AAO and negative PNA phases). This creates favorable conditions for high TC frequency in this region. In addition, as the anomalous pressure systems (SST) like High in South/Low in North (Low in South/High in North) in the western North Pacific intensify in these years, more TCs form in the northwestern region in the subtropical western North Pacific than in the low TC frequency years.

The MLRM developed in this study was for TCs that influence Taiwan during JAS. As seen in Fig. 1, the frequencies of TCs influencing Taiwan in June and October are relatively high as well. Therefore, we need to extend the prediction target season to include June and October (JJASO) and examine if the frequency of TCs influencing Taiwan during JJASO is also related to the two teleconnection patterns. In addition, the forecast performances of the MLRM developed in this study, the Poisson regression model, and the multivariate least absolute deviation model also need to be compared in future studies.

Acknowledgments This work is supported by NSC98-2111-M-002-008-MY3 and NSC100-2199-M-001-029-MY5.

References

Chan JCL, Shi JE, Lam CM (1998) Seasonal forecasting of tropical cyclone activity over the western North Pacific and the South China Sea. Wea Forecasting 13:997–1004

Chan JCL, Shi JE, Liu KS (2001) Improvements in the seasonal forecasting of tropical cyclone activity over the western North Pacific. Wea Forecast 16:491–498

Chen TC, Wang SY, Yen MC (2006) Interannual variation of the tropical cyclone activity over the western North Pacific. J Clim 19:5709–5720

Choi KS, Kim DW, Byun HR (2009) Statistical model for seasonal prediction of tropical cyclone frequency around Korea. Asia-Pac J Atmos Sci 45:21–32

Choi KS, Moon JY, Chu PS, Kim DW (2010) Seasonal prediction of tropical cyclone genesis frequency over the western North Pacific using teleconnection patterns. Theor Appl Climatol 100:191–206

Chu PS, Zhao X, Lee CT, Lu MM (2007) Climate prediction of tropical cyclone activity in the vicinity of Taiwan using the multivariate least absolute deviation regression method. Terr Atmos and Ocean Sc 18:805–825

Elsner JB, Liu KB (2003) Examining the ENSO-typhoon hypothesis. Clim Res 25:43–54

Elsner JB, Schmertmann CP (1993) Improving extended range seasonal predictions of intense Atlantic hurricane activity. Wea Forecast 8:345–351

Fan K, Wang HJ (2009) A new approach to forecasting typhoon frequency over the western North Pacific. Wea Forecast 24:974–986

Gong DY, Ho CH (2003) Arctic oscillation signals in the East Asian summer monsoon. J Geophys Res 108(D2):4066. doi:10.1029/2002JD002193

Gong DY, Wang S (1999) Definition of Antarctic oscillation index. Geophys Res Lett 26:459–462

Gray WM, Landsea CW, Mielke PW, Berry KJ (1992) Predicting Atlantic seasonal hurricane activity 6–11 months in advance. Wea Forecast 7:440–455

Gray WM, Landsea CW, Mielke PW, Berry KJ (1993) Predicting Atlantic basin seasonal tropical cyclone activity by 1 August. Wea Forecast 8:73–86

Gray WM, Landsea CW, Mielke PW, Berry KJ (1994) Predicting Atlantic basin seasonal tropical cyclone activity by 1 June. Wea Forecast 9:103–115

Hess JC, Elsner JB (1994) Historical developments leading to current forecast models of annual Atlantic hurricane activity. Bull Am Meteor Soc 75:1611–1621

Ho CH, Kim JH, Kim HS, Sui CH, Gong FY (2005) Possible influence of the Antarctic Oscillation on tropical cyclone activity in the western North Pacific. J Geophys Res 110: doi:10.1029/2005JD005766

Kalnay E, Kanamitsu M, Kistler R, Collins W, Deaven D, Gandin L, Iredell M, Saha S, White G, Woollen J, Zhu Y, Leetmaa A, Reynolds R, Chelliah M, Ebisuzaki W, Higgins W, Janowiak J, Mo KC, Ropelewski C, Wang J, Jenne R, Joseph D (1996) The NCEP/NCAR 40-year reanalysis project. Bull Am Meteor Soc 77:437–471

Kistler R, Kalnay E, Collins W, Saha S, White G, Woollen J, Chelliah M, Ebisuzaki W, Kanamitsu M, Kousky V, van den Dool H, Jenne R, Fiorino M (2001) The NCEP/NCAR 50-year reanalysis. Bull Am Meteor Soc 82:247–267

Klotzbach PJ (2007) Revised prediction of seasonal Atlantic basin tropical cyclone activity from 1 August. Wea Forecast 22:937–949

Kwon HJ, Lee WJ, Won SH, Cha EJ (2007) Statistical ensemble prediction of the tropical cyclone activity over the western North Pacific. Geophys Res Lett 34, L24805. doi:10.1029/2007GL032308

Lee WJ, Park JS, Kwon HJ (2007) A statistical model for prediction of the tropical cyclone activity over the western North Pacific. J Korean Meteorol Soc 43:175–183

Lehmiller GS, Kimberlain TB, Elsner JB (1997) Seasonal prediction models for North Atlantic basin hurricane location. Mon Wea Rev 125:1780–1791

Liu KS, Cahn JCL (2003) Climatological characteristics and seasonal forecasting of tropical cyclones making landfall along the South China coast. Mon Wea Rev 131:1650–1662

Lu MM, Chu PS, Lin YC (2010) Seasonal prediction of tropical cyclone activity in the vicinity of Taiwan using the Bayesian multivariate regression method. Wea Forecast 25:1780–1795

Lu MM, Lee CT, Wang B (2012) Seasonal prediction of accumulated tropical cyclone kinetic energy around Taiwan and the sources of the predictability. Int J Climatol. doi:10.1002/joc.3634 (online published)

Ramaswamy C, Pareek RS (1978) The southwest monsoon over Indian and its teleconnections with the middle and upper tropospheric flow patterns over the Southern Hemisphere. Tellus 30:126–135

Reynolds RW, Rayner NA, Smith TM, Stokes DC, Wang W (2002) An improved in situ and satellite SST analysis for climate. J Clim 15:1609–1625

Rodwell MJ (1997) Breaks in the Asian monsoon: the influence of Southern Hemisphere weather systems. J Atmos Sci 54: doi:10.1029/2005GL022419 2597–2611.

Rogers JC (1990) Patterns of low-frequency monthly sea level pressure variability (1899–1986) and associated wave cycle and frequencies. J Clim 3:1364–1379

Thompson DWJ, Wallace JM (2000) Annular modes in the extratropical circulation, part II: trends. J Clim 13:1018–1036

Velden CS, Leslie LM (1991) The basic relationship between tropical cyclone intensity and the depth of the environmental steering layer in the Australian region. Wea Forecast 6:244–253

Wallace JM, Gutzler DS (1981) Teleconnections in the geopotential height field during the Northern Hemisphere winter. Mon Wea Rev 109:784–812

Wang B, Chan JCL (2002) How strong ENSO affect tropical storm activity over the western North Pacific. J Clim 15:1643–1658

Wilks DS (1995) Statistical methods in the atmospheric sciences. Academic Press, San Diego, p 467

Wu MC, Chang WL, Leung WL (2004) Impacts of El Niño-Southern Oscillation events on tropical cyclone landfalling activity in the western North Pacific. J Clim 15:1419–1428

Xue F, Wang HJ, He JH (2004) Interannual variability of Mascarene High and Australian High and their influences on East Asian summer monsoon. J Meteorol Soc Jp 82:1173–1186

Zhou BT, Cui X (2008) Hadley circulation signal in the tropical cyclone frequency over the western North Pacific. J Geophys Res 113, D16107. doi:10.1029/2007JD009156

Zhou BT, Cui X (2011) Sea surface temperature east of Australia: a predictor of tropical cyclone frequency over the western North Pacific? Chinese Sci Bull 56:196–201